2019-24-0163 Published 09 Sep 2019

Heat Transfer Analysis of Catalytic Converters during Cold Starts

Viola Papetti and Panayotis Dimopoulos Eggenschwiler Empa

Augusto Della Torre, Gianluca Montenegro, and Angelo Onorati Politecnico di Milano

Grigorios Koltsakis Aristotle University Thessaloniki

Citation: Papetti, V., Dimopoulos Eggenschwiler, P., Della Torre, A., Montenegro, G. et al., "Heat Transfer Analysis of Catalytic Converters during Cold Starts," SAE Technical Paper 2019-24-0163, 2019, doi:10.4271/2019-24-0163.

Abstract

The transient heat transfer behavior of an automotive catalytic converter has been simulated with OpenFOAM in 1D. The model takes into consideration the gas-solid convective heat transfer, axial wall conduction and heat capacity effects in the solid phase, but also the chemical reactions of CO oxidation, based on simplified Arrhenius and Langmuir-Hinshelwood approaches. The associated parameters are the results of data in literature tuned by experiments. Simplified cases of constant flow rates and gas temperatures in the catalyst inflow have been chosen for a comprehensive analysis of the heat and mass transfer phenomena. The impact of inlet flow temperatures and inlet flow rates on the heat up characteristics as well as in the CO emissions have been quantified. A dimensional analysis is proposed and dimensionless temperature difference and space-time coordinates are introduced. Using this suitably modified coordinates, for the case of negligible axial solid conduction, computed solid temperature at the reactor outlet lay on a typical S-curve, allowing the introduction of an analytical function. A series of variations in the inlet exhaust temperature and mass flow as well as the initial solid temperature was chosen in order to highlight relevant dependencies. Results show the performance of the catalyst during cold start and have been used for a preliminary energetic assessment of the effectiveness of preheating the catalyst, the exhaust gas or both.

Introduction

Emissions of Euro 6c/d-gasoline vehicles at normal operating temperature are very low. Exception is the cold start and warming up phase. CO, unburned hydrocarbon (HC) and NOx emissions are 2-3 orders of magnitude higher during this phase. According to the emissions inventory program [1], cold start emissions of Euro 5 passenger cars amount to 68% of their total CO and 88% of HC emissions. Literally, modern engines emit during cold start the pollutant amount they would emit over more than 1'000km of warm operation [2]. Newest targeted measurements and simulations performed in our laboratory on a Euro 6 gasoline vehicle have shown that 17% of the CO, 91% of the THC and 66% of the NOx emissions during the WLTC cycle happen in the first 300s after the engine cold start (20°C). This is due to the chemical reaction mechanism, strictly related to temperature. When engine is switched on, cold aftertreatment systems are not able to start the reactions.

Moreover, all newest engine concepts are oriented towards maximizing engine efficiency and thus minimizing fuel consumption and CO emissions. Increased engine efficiency has as consequence decreasing engine exhaust temperatures (1st law of thermodynamics). Thus, all near-future powertrain concepts will face increasing difficulties conflicting with the fuel saving imperative in providing the necessary temperatures for the pollutant aftertreatment. These will affect primarily cold start and low-load operation, typical for instance in city driving. The situation is even more severe with hybrid powertrains. Here the intermittent engine operation often leads to numerous cold starts.

Thus, it is important to understand and control the cold start behavior of after-treatment systems, the complex transient phenomena related to heat and mass transfer and to reaction activities.

Previous work of the group has focused in detail on characterizing cold start phenomena, [3]. Complete cold-start transients for catalytic converters have been simulated on fine length scales for different geometries, washcoat parameters, CO inflow mass fractions and inflow velocities. Mathematical models simulating the thermal and chemical phenomena in the monolithic converter have been developed to assess different monolithic geometries at specified operating conditions such as a step increase in inlet gas temperature and flow rate [4] or transient operation occurring during cold-start phase of legislated driving cycles [5]. Heat and mass transfer with dimensionless analysis has been proposed in [5, 6]. In [5] a non dimensional approach is adopted in order to describe the heat up inside a channel of the monolithic structure. [6]

describes an appropriate model capable of predicting multiple steady states occurring in monolithic structures and proposes numerical techniques for solution of this model. However, up to now, the investigation has been under limited steady state conditions, considering temperature behaviour only at inlet and outlet positions.

In this work, the thermal transient problem has been solved along the entire length of the monolithic catalytic converter and the analysis is extended to species concentration. OpenFOAM simulations investigate the behavior of the catalytic converter along its entire length during the first 400s of operation and compare different fluid and solid properties for deriving best practice for reducing cold start emissions. To be precise, the effects of different mass flows, temperatures of the fluid entering the catalytic converter, initial solid temperatures have been investigated. Moreover, results have been analysed at different positions along the catalytic converter: at the end, but also at ½, ¼ and ¾ of the length. An analytical model and dimensional analysis has also allowed to derive global solutions, able to avoid extra experiments, simplifying simulations and to reveal simpler relations of the interactions of the important parameters.

Methodology

The configuration of a monolithic honeycomb catalyst substrate with real size vehicle dimensions has been simulated with OpenFOAM in order to study the mechanisms of heat transfer during cold starts. In the scale of a single channel of the honeycomb structure an "analytical" approach has been introduced by means of simplified differential equations. Data from the detailed simulation have been used in order to access the inaccuracy introduced by the simplified approach. The equations are reported below. The analytical model has been compared to the simulations as well as relevant results from literature.

Analytical Model Equations and Assumptions

The model is of a single channel inside the monolithic configuration and takes into account the gas-solid convective heat and mass transfer, longitudinal thermal conductivity and heat capacity effects in the solid phase. The model neglects the radial variations of the gas-phase temperature, concentration, and velocity within the channel so that these variables are to be interpreted as cross-sectional averages. Accumulation of mass and heat in the gas phase is neglected (fluid time constants are typically much smaller than that of the solid thermal response [8]). This implies quasi-steady state condition for the fluid phase considering temporal changes only characteristics for the solid. The wall heat capacity is large compared with the heat capacity of the fluid. Thus, during a small time increment, only the effect of varying wall temperature needs to be taken into account and the fluid heat capacity effect can be ignored [8]. Heat transfer to the ambient in the warm up phase was considered as negligible, since during warm up, temperature difference between the catalytic converter and the ambient are small. The channel is considered to be initially at a constant temperature, $T_S(t=0)=T_0$, the feed gas enters the duct at a constant inlet temperature T_{Fin} ($T_{Fin} > T_S$) and constant mass flow $\dot{m}_F$. The analysis will focus on the temporal evolution of the solid and fluid temperature at different positions along the catalytic converter. T_F and T_S are function of time and space. Assuming quasi-steady state, incompressible flow, considering an infinitesimal volume of the fluid phase (see Fig. 1), the energy balance can be formulated as:

FIGURE 1 Schematic of the analytical model.

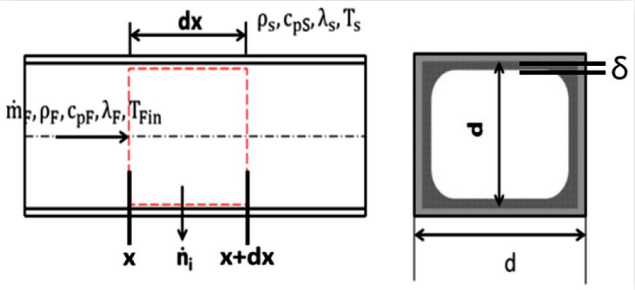

$$\dot{m}_F c_{PF} \frac{\partial T_F}{\partial x} dx = -\alpha A_{//} \left(T_F - T_S \right) \quad (1)$$

$A_{//}$ represents the liquid-solid interface, thus the lateral surface of the reference infinitesimal volume. $\dot{m}_F$ is the fluid mass flow and c_{PF} the fluid specific heat capacity. α is the convection coefficient. Considering the definition of Nusselt number $Nu = \frac{\alpha\, dx}{\lambda_F}$, Eq. (1) becomes:

$$\dot{m}_F c_{PF} \frac{\partial T_F}{\partial x} = -4 Nu \lambda_F \left(T_F - T_S \right) \quad (2)$$

Due to the monolithic geometry, the flow and thermal boundary layers are fully developed over the largest part of the reactor. Thus, the heat transfer augmentation due to flow entrance effects is not considered and a constant Nu is considered for the entire channel length. The equation can also be written as:

$$\frac{\partial T_F}{\partial x} = -\frac{4 Nu \lambda_F}{\dot{m}_F c_{PF}} \left(T_F - T_S \right) \quad (3)$$

The energy balance in the solid phase in 1D infinitesimal mesh (see Fig. 1) can be written as:

$$\dot{Q}_{x+dx} - \dot{Q}_x - \alpha A_{//} \left(T_F - T_S \right) + \Delta \dot{H}_R = m_S c_S \frac{\partial T_S}{\partial t} \quad (4)$$

$\alpha A_{//}(T_{F,x,t} - T_{S,x,t})$ represents the convective term, while ΔH_R represents the heat related to chemical reactions. Considering the enthalpy released by reactions as small (valid only for the heat up cases examined in this study), ΔH_R is neglected. The definition of Nu is used. Eq. (4) becomes:

$$m_S c_S \frac{\partial T_S}{\partial t} = \lambda_S A_{S,FRONT} \frac{\partial^2 T_S}{\partial x^2} dx - \frac{Nu \lambda_F}{d} A_{//} \left(T_F - T_S \right) \quad (5)$$

Considering Eq. (3) and (5), the solid energy balance becomes:

$$\frac{\partial T_S}{\partial t} = \frac{\lambda_S}{\rho_S c_S}\frac{\partial^2 T_S}{\partial x^2} + \frac{\dot{m}_F c_{pF}}{A_{S,FRONT}\,\rho_S c_S}\frac{\partial T_F}{\partial x} \tag{6}$$

Similarly we can proceed with the mass transfer from the bulk to the walls. The species mass conservation in an infinitesimal fluid volume (Fig. 1), with CO as a specie is:

$$\left(u_\infty c_{CO_{x+dx}} - u_\infty c_{CO_x}\right) d^2 \frac{\rho_F}{M_F} = \dot{n}_{CO} dx\, d^2\, 4 \tag{7}$$

Eq. (7) simply represents the fact that the difference between what exits and enters the infinitesimal control volume correspond to the mass transfer to the walls. c_{CO} represents the CO species concentration expressed in $\left[\frac{mol_{CO}}{mol_{TOT}}\right]$ and $\dot{n}_{CO}$ is the reaction rate of species CO $\left[\frac{mol_{CO}}{s\,m^3}\right]$. $\dot{n}_{CO}$ is defined as:

$$\dot{n}_{CO} = -\frac{k_{CO}\,\rho_F}{M_F\,d}\left(c_{CO,F} - c_{CO,S}\right) \tag{8}$$

With k_{CO} as the CO mass transfer coefficient:

$$k_{CO} = \frac{Sh\, D_{CO}}{d} \tag{9}$$

Substituting Eq. (8) and (9) in (7), it is obtained:

$$\frac{\partial c_{CO,F}}{\partial x} = -\frac{4\,Sh\,D_{CO}\rho_F}{\dot{m}_F}\left(c_{CO,F} - c_{CO,S}\right) \tag{10}$$

Simulation Model

A monolithic honeycomb catalyst substrate has been simulated with OpenFOAM. The system of energy, mass, momentum and species differential equations has been modelled and solved [9]. The model is 1D and takes into consideration the gas-solid convective heat transfer, axial wall conduction and heat capacity effects in the solid phase. Chemical reactions have also been modelled based on simplified Arrhenius and Langmuir-Hinshelwood approaches. The associated parameters have been chosen by tuning experimental data starting from literature data taken from [10, 11, 12]. Up to now, CO oxidation has been taken into account under oxygen abundance, i.e., typical Diesel Oxidation Catalyst conditions. The model adopts a double phase macroscale approach. Thus, geometry of the solid phase is modelled with lumped parameters, such as Sv, ε. The material is the conventional, well known cordierite. Models of heat and mass transfer of honeycomb catalytic converter have been taken from literature [13]. Due to the very dense cell structure of monoliths and the special geometrical characteristics (large length compared to the hydraulic diameter of the channels), the flow can be considered as laminar and developed.

Different configurations have been simulated with the same monolithic geometry. The parameters varied have been the fluid temperature at the inlet of the converter TFin(x=0), the temperature of the solid (catalytic converter) at the initial time instant TS(t=0) and the fluid velocity, respectively the fluid mass flowrate. A pre-study revealed the fluid temperature range of particular interest. TFin should be at typical cold-start levels while neither being too low (time for converter heat up increases exponentially) neither too high, where catalytic converter heat up is extremely fast. The characteristics in focus have been the temperatures and CO concentrations of the fluid and the solid as a function of time and space during the first 100-500s after cold start.

For the sake of simplicity, we have extracted the results of fluid and solid phase at five different positions along the mesh length: these correspond to inlet (x=0), one quarter of the length, (x=¼L=0.038m), half of the length, (x=1/2L=0.076m), three quarters of the length, (x=3/L =0.1148m) and exit length (x=L=0.1524m).

Dimensionless Quantities and Approximation Possibilities

By introducing dimensionless quantities, the possibility of deriving analytical solutions as well as some approximations is given. The approach followed is based on concepts introduced in heat transfer [14], as well as in [5, 7, 15]. In Eq. (3) and (6) a dimensionless temperature difference can be introduced according to Eq. (12) and (13) and based on the well established heat transfer approach, [14]. It is important to notice that T_F and T_S are function of time and space, thus even θ_S and θ_F are function of time and space:

$$\theta_S = \frac{T_S - T_0}{T_{F,in} - T_0} \tag{11}$$

$$\theta_F = \frac{T_F - T_0}{T_{F,in} - T_0} \tag{12}$$

The reference temperature was chosen for simplicity as the initial solid temperature. Dimensionless fluid temperature represents the ratio between the instantaneous solid-fluid temperature difference and the initial solid-fluid temperature difference. Under the hypothesis of negligible reactions, which is true in the first period of the simulations, dimensionless solid temperature represents the increment of solid temperature with respect to the maximum increment it can reach, which is exactly the initial fluid-solid temperature difference. A dimensionless length, ξ, similarly to [7], can be introduced, as:

$$\xi = \frac{4Nu\lambda_F x}{\dot{m}_F c_{PF}} = NTU_\theta \tag{13}$$

Clearly, ξ, corresponds to the number of transfer units NTU_θ. Moreover, according to [7], a dimensionless time can be introduced:

$$\tau = \frac{4Nu\lambda_F t}{A_{S,FRONT}\,\rho_S c_S} \tag{14}$$

Based on Eqs. (11)-(14), Eq. (3) and (6) can be rewritten as:

$$\frac{\partial \theta_F}{\partial \tau} = \theta_S - \theta_F \tag{15}$$

$$\frac{\partial \theta_S}{\partial \tau} = \frac{4Nu\lambda_F A_{S,FRONT}\,\lambda_S}{\dot{m}_F{}^2 c_{PF}{}^2}\frac{\partial^2 \theta_S}{\partial \xi^2} + \frac{\partial \theta_F}{\partial \xi} \tag{16}$$

with

$$Nu = 2.976\left(1 + 0.078 Re_d Pr \frac{d}{L}\right)^{0.45} \tag{17}$$

In Eq. (6), the coefficient of the term of the second derivative of Ts with respect to spatial coordinate x can be summarized by dimensionless heat conductivity, Λ, [7]:

$$\Lambda = \frac{4Nu\lambda_F A_{S,FRONT}\,\lambda_S}{\dot{m}_F{}^2 c_{PF}{}^2} \tag{18}$$

Eq. (16) can be rewritten as:

$$\frac{\partial \theta_S}{\partial \tau} = \Lambda \frac{\partial^2 \theta_S}{\partial \xi^2} + \frac{\partial \theta_F}{\partial \xi} \tag{19}$$

It should be noted that the dimensionless solid temperature compares the difference between fluid and solid temperature with respect to the difference between the fluid inlet and the initial solid temperatures. The dimensionless time compares the rate at which heat is convected from fluid to solid and the rate at which heat is stored in the solid (compares the diffusive transport rate and the storage rate) while the dimensionless length compares the convection capacity and the storage capacity of the fluid.

We can proceed similarly with the mass transfer equation (10). Considering also a non dimensional species space coordinate defined as:

$$\xi_{CO} = \frac{4\,Sh\,D_{CO}\rho_F x}{\dot{m}_F} = NTU_m \tag{20}$$

Thus, eq. (10) can be rewritten as:

$$\frac{\partial c_{CO,F}}{\partial \xi_{CO}} = -\left(c_{CO,F} - c_{CO,S}\right) \tag{21}$$

The similarity between Eq. (15) and (21) is obvious.

In [5, 7, 15] the equations are solved by assuming a series of quasi steady states. This is the case when during a single time step, the temperature of the solid phase can be taken as constant. The first operation is the computation of the fluid temperature along the entire catalytic length in the time step considered. This implies the calculation of temperature T_F at node i+1 based on the known fluid and solid temperatures in the previous location i. Eq. (15) can be solved according to:

$$T_{F,i+1,t} = T_{S,i,t} + \left(T_{F,i,t} - T_{S,i,t}\right)e^{-NTU_\theta} \tag{22}$$

The convective heat per unit volume exchanged at each location can be obtained by:

$$\dot{q}_{conv,i,t} = \frac{\dot{m}_F c_{PF}}{\Delta V}\left(T_{F,i,t} - T_{S,i,t}\right)\left(1 - e^{-NTU_\theta}\right) \tag{23}$$

Similarly, the computation of the concentration in the fluid in the next spatial increment (i+1) is given by solving Eq. (21). The expression becomes:

$$c_{CO,F,i+1} = c_{CO,S,i} + \left(c_{CO,F,i} - c_{CO,S,i}\right)e^{-NTU_m} \tag{24}$$

The local molar flux for each species at the wall is:

$$\dot{n}_{CO,i} = \frac{\dot{m}F}{M_F \Delta V}\left(c_{CO,F,i} - c_{CO,S,i}\right)\left(1 - e^{-NTU_m}\right) \tag{25}$$

The chemical reaction rates and species concentrations at the gas-solid interface can be computed by equating the diffusion, Eq. (8), and the reaction rates for the species under consideration.

$$\frac{k_{CO}\,\rho_F}{M_F\,d}\left(c_{CO,F,t} - c_{CO,S,t+dt}\right) = k_1 c_{CO,S,t+dt} c_{O_2,S,t} \tag{26}$$

Already for the species under consideration CO, the reaction rate-diffusion equilibrium (Eq. (26)) requires the simulation of an additional species balance, i.e. of O_2. This is indicative for the complexity of multiple reaction modelling. In the present study, only CO oxidation under oxygen abundance (typical Diesel Oxidation Catalyst conditions) is taken into account. In TWC applications, the oxygen storage and release have also to be formulated. In Eq. (26) k1 is temperature dependent ($T_{S,i,t}$) since modelled with Langmuir-Hinshelwood approach.

The final step is the computation of the solid temperature in time t+dt. As long as the reaction rate energy release is low, this can be done by solving Eq. (19). [7] introduced the possibility for a solution based on a semiempirical-analytical approach. In the present work we comment on that with Fig. 9. Should the energy released by the chemical reactions not be negligible, then Eq. (4) has to be solved.

Results and Discussion

Temporal Evolution of Temperature inside the Catalytic Converter

Fig. 2 represents the fluid and solid phase temperature time histories at the different local positions as described. The results correspond to the case of fluid entering with T_{Fin}=410K, $\dot{m}_F$=0.0043kg/s, while two different T_S(t=0) have been chosen 260K in a) and 360K in b). In all the figures, solid lines represent the temperature of the fluid while dashed lines the temperature of the solid.

In the entrance of the catalyst, the fluid is instantly cooled down, to a temperature of 350K in a) and 390K in b) resulting based on the thermal effusivities involved. Thereafter (still taking the entrance only into account) fluid and solid heat up, until the temperature of the fluid reassumes its inflowing temperature and the temperature of the solid reaches the temperature of the fluid. As the gas flows through the downstream catalyst parts, it is further cooled down towards the solid initial temperatures. So, for t<30s, T_F(x=1/4L)=T_S(t=0)

FIGURE 2 Fluid (solid lines) and catalyst (dashed lines) temperature time histories in different locations inside the catalytic converter, T_{Fin}=410K and $\dot{m}_F$ =0.0043kg/s, T_S(t=0)=260K in (a) and 360K (b).

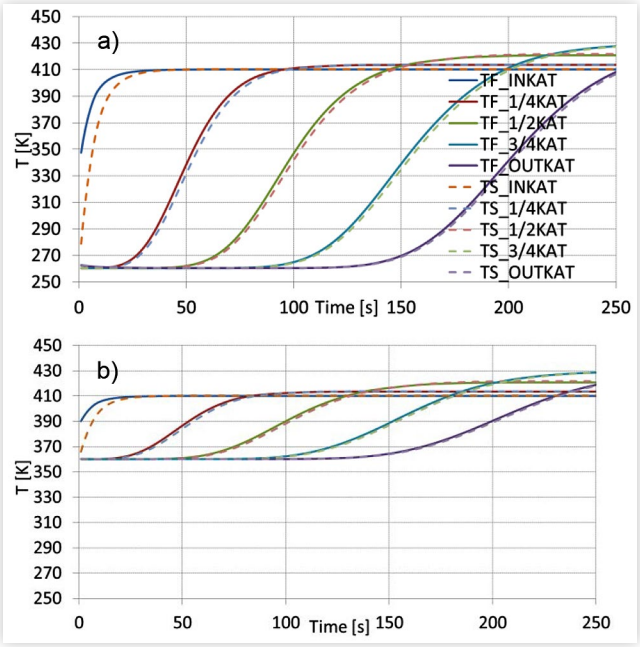

and in a similar manner for t<50s T_F(x=1/2L)=Ts(t=0) as well as for t<100 T_F(x=3/4L)=T_S(t=0).

The following insights can be summarized from Fig. 2:

- At the beginning (t<30secs) the gas warms up the catalytic converter entrance and is rapidly cooled down in the downstream, reaching T_F(x>1/4L,T<30s)=T_S(t=0) already after the first quarter of the catalyst.
- Around t~30s, the very entrance of the catalytic converter (first dashed yellow line) reaches T_{Fin}, while the first quarter of the catalytic converter has started to warm up. At this time the catalytic converter temperature at half of the length has not yet changed, while the gas flowing though this and further downstream locations has assumed the (low) solid temperature (T_F(x>1/4L, T<30s)=T_S(t=0)).
- Temperature differences between solid and fluid decrease with time, they are significant in the first half of the converter and are very small in the second half.
- Before any reactions start, the temperatures are limited between T_S(t=0) and T_{Fin}.

First oxidation reactions occur in the very first part of the catalytic converter (as can be seen more clearly later in Fig. 10) while the heat generated is transported downstream, contributing to a somehow faster heat up of the downstream catalyst sections. First occurrence of T_S=T_F>T_{Fin} can be seen at x=1/4L and t>100s.

It is evident that the different T_S(t=0) in the examined cases do not affect the nature of the heat transfer mechanism. As can be seen by comparing Fig. 2 a) and b), higher T_S(t=0) only slightly accelerates the warm up process. In case b) the

FIGURE 3 Fluid (dashed curves) and catalytic converter (solid curves) temperature time histories in different locations inside the catalyst, T_{Fin}=410K, $\dot{m}_F$ = 0.0086kg/s, TS(t=0)=260K.

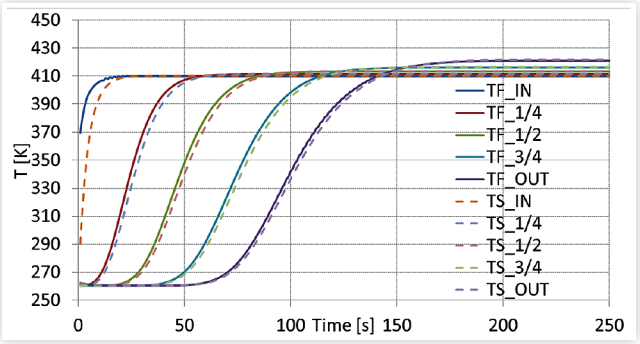

catalyst is warmer at the beginning, but the driving temperature differences to the gas is lower.

Fig. 3 describes the time history of the fluid and solid temperatures of the same setup of Fig. 2a, having though the double $\dot{m}_F$. Due to the higher fluid velocity, the heat transfer is stronger and there is a faster solid heat up. The general observations are the same as in Fig. 2, only with shorter time scales.

Introducing the dimensionless temperature difference according to Eq. (11), solid temperatures of Fig. 2 (case with T_{Fin}=410K and flow rate 0.0043kg/s) are plotted in Fig. 4 in function of dimensionless time, τ, according to Eq. (14). In addition, the case of T_S(t=0)=300K, together with the cases of Fig. 2 with T_S(t=0)=260K and 360K, has been considered (solid lines for T_S(t=0s)=260K, dashed lines for T_S(t=0s)=300K and thin dashed lines for T_S(t=0s)=360K).

θ_S is initially 0 (T_S=T_S(t=0s)), approaches unity when T_S = T_{Fin}. T_S>T_{Fin} due to the heat release by the onsetting oxidation reactions. The lines have all the characteristic S-type shape. As long as no reactions take place, the dimensionless time histories overlap at each location along the catalytic converter. This display highlights clearly the onset of oxidation reactions. Substantial deviation of single lines from other overlapping lines at each coordinate chosen, evidence the onset of the reactions. As expected, earliest oxidation reactions can be evidenced in the case with the highest catalyst

FIGURE 4 θ_S in function of τ in different locations inside the catalytic converter, T_{Fin} =410K and T_S(t=0)=(260,300,360)K.

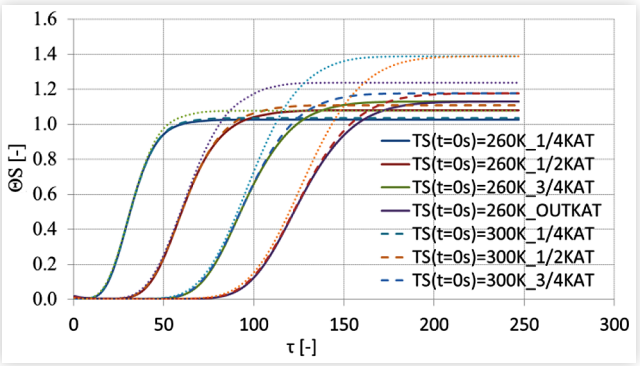

FIGURE 5 Dimensionless coordinate ξ in function of dimensional space coordinate x and the different flow and temperature parameters examined.

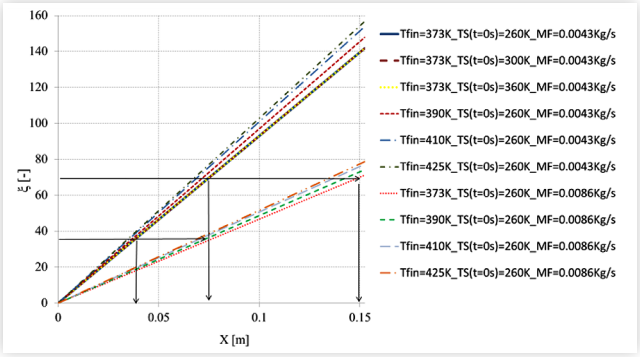

initial temperature, T_S(t=0)=360K (dashed lines in Fig. 4). By introducing θ_S, the effect of the initial solid temperature is compensated (as long as no chemical reactions release enough heat). It is important to highlight that each line is characterized by a specific value of x and thus by a dimensionless coordinate, ξ (according to Eq. (13)), and the groups of lines overlapping have not only the same τ, but also the same ξ (same T_{Fin}, $\dot{m}_F$ and x coordinate along the catalytic converter).

For clarity, in Fig. 5, the trend of ξ along the catalytic converter length can be seen for different fluid flow and property configurations. The relationship between dimensional x and dimensionless ξ is linear as can be seen also by Eq. (13). The steepness of the lines is a function of $\dot{m}_F$ and T_{Fin}. T_S does not influence ξ, (also evident from Eq. (13)). In fact, ξ profiles with the same T_{Fin}=373K and $\dot{m}_F$=0.0043kg/s, but different T_S(t=0s)=(260, 300, 360)K, overlap. Instead, by increasing T_{Fin}, the curve steepness slightly increases. Moreover, $\dot{m}_F$ has a strong impact (influences also Nu) and at constant T_{Fin}, at the same space coordinates, the higher $\dot{m}_F$, the lower is ξ. Intuitively, it can be thought that a stronger flow heats up each catalytic converter part faster. It is also interesting to notice that the same ξ may correspond, for instance, to situations with same T_{Fin}, different $\dot{m}_F$, at different x positions: in Fig. 5, with a black line, the same ξ corresponds to the ¼L position with T_{Fin}=373K and $\dot{m}_F$=0.0043kg/s, but also to ½ L with same T_{Fin} and double mass flow. The same consideration is valid if we consider position ½ L and entire L respectively. These observations evidence the similarity of all the cases examined.

Certainly, of importance is to investigate the effect of different T_{Fin} and different $\dot{m}_F$ on the temperature profile in time and space. Due to the analogy found in Fig. 4, a dimensionless approach has been adopted. The similar sets of lines presented in Fig. 4 are reported for different T_{Fin} in Fig. 6a and for different $\dot{m}_F$ in Fig. 6b. For simplicity of the figures, only one value of T_S(t=0s)=260K has been considered. In Fig. 4 it is evident that besides the dimensionless time, τ, the characteristic parameter is the dimensionless space coordinate, ξ: each line is in fact characterized by a specific value of ξ. For instance, in Fig. 6a, considering the behavior before reactions start, all the curves corresponding to the same spatial coordinate along the catalytic converter with different T_{Fin}, are almost overlapping. The slight differences are due to slightly

FIGURE 6 θ_S in function of τ in different locations inside the catalytic converter. Ts(t=0)=260K, with different T_{Fin} = (373, 390, 410, 425)K and identical $\dot{m}_F$=0.0043kg/s (a), and with one T_{Fin} =410K but with two different $\dot{m}_F$ =(0.0043, 0.0086) kg/s (b).

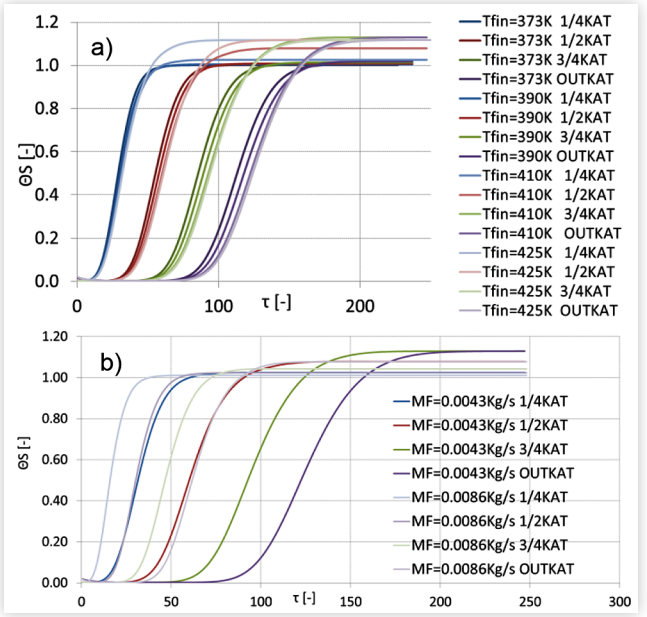

different ξ (T_{Fin} slightly influences ξ, since it changes Re which in turn is used for the estimation of the Nu number, Eq. (17)). In the same way, in Fig. 6b, the dimensionless time is not able to scale different mass flow rates: curves of different mass flow rates corresponding to the same space position along the catalytic converter do not overlap due to different ξ. However, due to the nature of some of the values chosen for the compared flowrates ($\dot{m}_{F2}$=0.0086kg/s= 2$\dot{m}_{F1}$=0.0043kg/s) there are lines overlapping due to corresponding same ξ: this is the case of simulations with 0.0043kg/s at ½ L and with double flow rate (0.0086kg/s) at L, or also the case of 0.0043kg/s at ¼L and with 0.0086kg/s at ½ L.

Spatial Distribution of Temperature inside the Catalytic Converter

For reactions to start, sufficient high temperatures are required in specific localized points inside the catalytic converter and not in the entire solid phase. In Fig. 7 the data presented are identical to Fig. 4, but this time the temperature differences are plotted over the space coordinate in four different time instants. Fig. 7a represents the temperature profile along the catalytic converter length at different time instants. It is clear that the fluid is cooled down along the flow through the catalytic converter, while warming the solid (catalytic converter) up; the effects are already evident from the beginning in the first catalyst half, and much more pronounced but later in the second half. At t=50s the first half of the catalyst is been gradually warmed up, while the second half still has the initial temperature.

FIGURE 7 Solid temperature profile along the catalyst length at different time instants (a) and the corresponding figure in non dimensional quantities (b), T_{Fin} =410K and $T_S(t=0)$=(260,300,360)K.

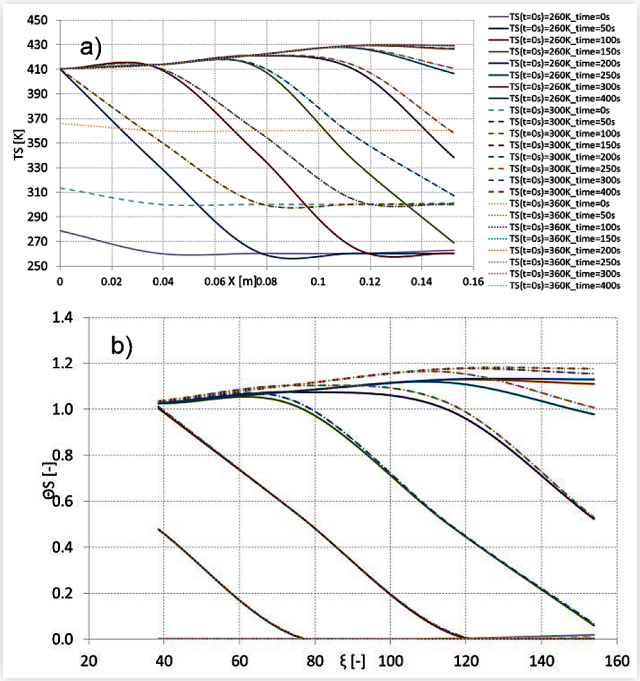

Temperatures higher than T_{Fin} are due to exothermic chemical reactions: first reactions are evident very soon in the entrance region, while much later in the downstream catalyst parts. The impact of different $T_S(t=0s)$ is evident in the first 150s, and it decreases with time: in fact, in the first time span, the temperature gradients along the catalytic converter are higher in the case of the lower $T_S(t=0s)$, but the final temperature profiles are almost independent from $T_S(t=0s)$.

With the dimensionless approach, instead, Fig. 7b presents θ_S in function of ξ at different time instants. The lines corresponding to different $T_S(t=0s)$ at the same time instant overlap perfectly, till reactions take place. The profiles that overlap correspond to the same τ. This means that the dimensionless time is also a characteristic property to take into consideration. The effects of reactions increase in the case of higher $T_S(t=0s)$. The steepness of the lines decrease over time due to the reduction of the temperature gradient between solid and fluid, till the temperature profile inside the catalytic converter is homogeneous.

The same sets of lines presented in Fig. 7b are shown for two different T_{Fin} in Fig. 8a and for two different $\dot{m}_F$ in Fig. 8b. Fig. 8a represents θ_S profiles along ξ at different time instants for different T_{Fin}. The impact of different T_{Fin} is low till reactions start; the two lines corresponding to the same time instant slightly differ, given that the dimensionless time is slightly different (T_{Fin} influences Nu). At the lower T_{Fin} =390K, only a small part of the CO reacts, so θ_S only slightly exceeds 1 (which correspond to $T_S>T_{Fin}$).

Fig. 8b highlights instead the influence of different $\dot{m}_F$: The θ_S profiles along ξ are plotted for different time instants for the case of T_{Fin} =410K, $T_S(t=0s)$=260K, while varying $\dot{m}_F$.

FIGURE 8 θ_S in function of ξ at different time instants with $T_S(t=0)$=260K, with T_{Fin}=(390,410)K, $\dot{m}_F$=0.0043kg/s in Fig. 8a and with T_{Fin}=410K, $\dot{m}_F$=(0.0043, 00086)kg/s in Fig. 8b.

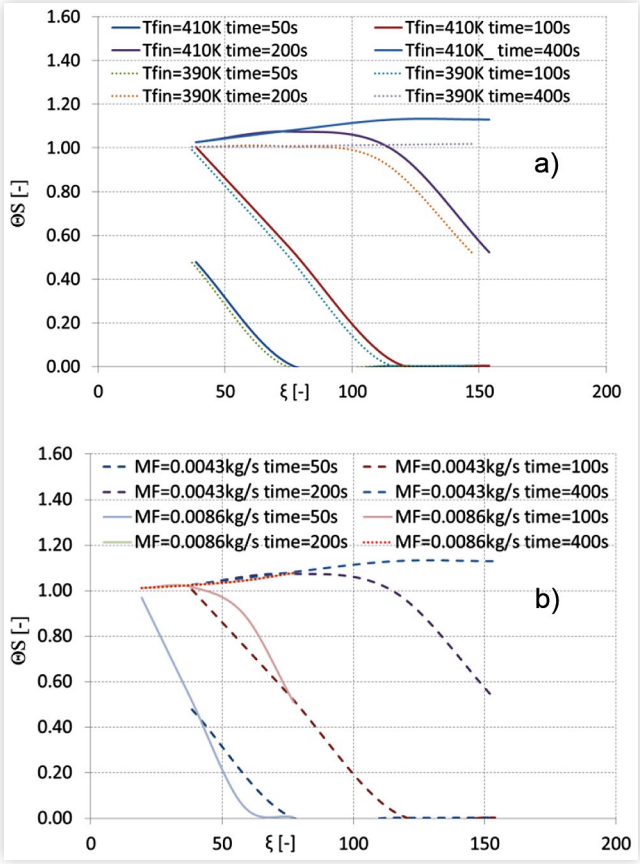

Consequently, the characteristic ξ range varies (ξ depends on $\dot{m}_F$, higher $\dot{m}_F$ means lower ξ, see Fig. 5). ξ varies within [38.48, 153.92] with $\dot{m}_F$=0.0043kg/s, and within [19.32, 76.96] with the double $\dot{m}_F$. Higher $\dot{m}_F$ implies higher steepness of the lines and faster heat up. All the lines differ due to different τ coordinates.

Characteristics of the Instationary Heat Transfer

In the non dimensional approach of Fig. 6, θ curves over τ do not overlap due to different ξ. Similarly, in Fig. 8, θ trends in function of ξ do not overlap due to different τ. In [7], the response of the temperature of a monolithic converter in the solid phase was introduced as a function of τ/ξ. Fig. 9 shows the profile of θ_S in function of τ/ξ for different setups (varying T_{Fin}, $T_S(t=0s)$ and $\dot{m}_F$). The characteristic S-type shape is clearly recognized for all the lines. The initial θ is 0 (θ_S=0, T_S= $T_S(t=0s)$) and approaches unity (T_S= T_{Fin}). Each line is characterized by a specific value of ξ, thus all the lines differ for the value of ξ, while higher ξ implies either larger space coordinate along the catalytic converter length at constant $\dot{m}_F$, or lower $\dot{m}_F$ at the same physical length. Lines corresponding to higher ξ are steeper. This leads to the conclusion that downstream parts of a catalyst are heated up later, but faster. Similar is the case with lower exhaust gas mass flows.

FIGURE 9 θ_S in function of τ/ξ, with Ts(t=0)=260K, T_{Fin} =(390,410)K, $\dot{m}_F$=0.0043kg/s and with T_{Fin} =410K, $\dot{m}_F$=(0.0043, 00086)kg/s.

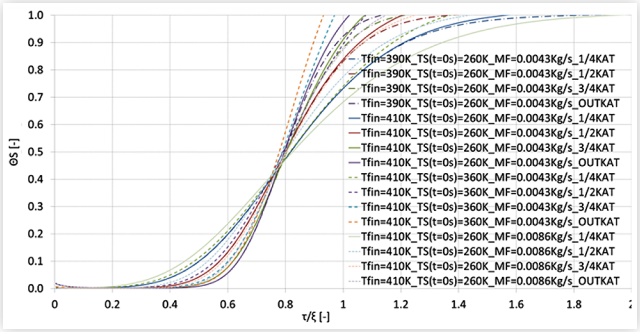

In addition, all the curves intersect in a single point corresponding to τ/ξ around 0.78, where the corresponding θ_S value is around 0.45.

Thus, the response of a monolithic converter is mainly governed by the parameter τ/ξ. Independently of the value of ξ, the value of the dimensionless temperature is 0.45 for τ/ξ close to 0.78. The values we found differ, but not significantly, from the ones reported in [7]. The heat up of a converter can be approximated by an analytical term using a double exponential function of the type:

$$\theta = \theta\left(\tau/\xi\right) = 1 - \exp\left(-k\left(\tau/\xi\right)^m\right) \tag{27}$$

Given the differences in the steepness of the lines in Fig 9, the exponent m should be a function of ξ, since this steepness of the lines is directly given by m.

The implications of Eq. (27) are of some interest for simplifying the numerical approach. First of all, it is clear that an equation similar to Eq. (27) can only describe the phenomena with some accuracy when the second term of Eq. (19) $\Lambda \frac{\partial^2 \theta_S}{\partial \xi^2}$ is small relatively to the third $\frac{\partial \theta_F}{\partial \xi}$ (and at negligible heat release through chemical reactions). This is the case when Λ is small, thus small or negligible axial heat conduction in the solid. This is also the case for the catalyst in question (ceramic material) at the present work having very low thermal conductivity (it is not the case when considering metallic catalyst substrates). In addition, Eq. (27) gives an analytical solution of the time and location dependent temperatures, should m and k be known. So by knowing m and k (through either previous simulations or experiments) the analytical solution provided by Eq. (27) can simplify the computations and the numerical solution of Eq. (19) is not necessary any more.

Fig. 10 shows the heat exchanged between fluid and solid over time in the four catalyst quarters as computed using Eq. (23) for three of the different cases examined up to now. The values are expressed per unit of volume. The case of T_{Fin} =390K, T_S(t=0s)=260K, the case of T_{Fin} =410K, T_S(t=0s)=260K and the one of T_{Fin} =390K, T_S(t=0s)=300K have been considered. As expected, in all the three different cases, the highest amount of heat is exchanged in the first catalyst quarter and the exchanged heat is decreasing further downstream.

FIGURE 10 Heat rate exchanged between the fluid and the solid, as integrated over the four catalyst parts.

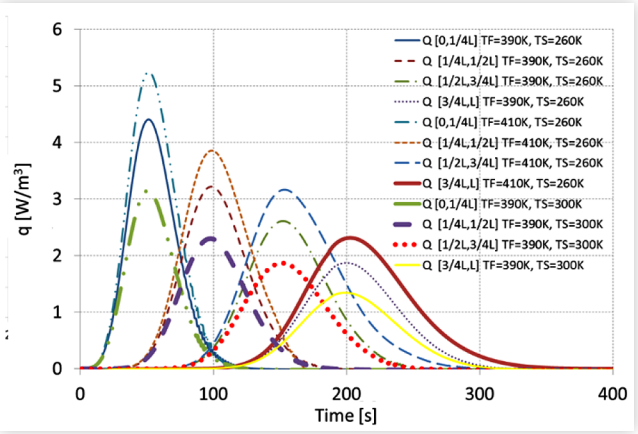

The case with the highest temperature difference between the fluid and the solid, i.e. T_{Fin}=410K and T_S=260K, is associated with the highest heat transfer rates.

Species Concentration in Time along the Catalytic Converter Length

Apart from the convective heat exchange between the exhaust gas and the substrate, heat is additionally generated by the first exothermic reactions at the catalytic active centres. Thus, it is important to understand the reaction mechanisms during cold start, also in order to design specific cold start measures (active catalyst heating) for reducing emissions. Fig. 11 describes both temperature and mass CO concentrations in time at the already described five different space positions along the catalytic converter. T_S(t=0s)=260K, $\dot{m}_F$=0.0043kg/s and T_{Fin} =390K in (a) while T_{Fin} =410K in (b). The dependence of CO concentration from the evolving (increasing) solid temperature is evident. Independently of T_{Fin}, reactions start only slightly before 20s when T_S reaches circa 385K. This is clearer in Fig. 11 which is a zoom in the first 150s of Fig. 10. The first oxidation reactions can be evidenced slightly before t=20s, where the CO concentration in the first quarter of the catalyst starts decreasing, falling below the CO concentration in the inlet. The CO concentration in the remaining catalyst parts (all along t<80s) is identical with the CO concentration in the first quarter, evidencing that no reactions happen in the downstream catalyst parts yet. This is consistent with the low temperature at these parts. At about t=80s the temperature in the first quarter of the catalyst stabilizes, and the reaction rate of CO oxidation stabilizes as well, while, consequently, the CO concentration (at x=1/4L) remains constant. The further decrease of the CO concentration in the next quarter of the catalyst evidences the onset of the reactions here. The reaction rate in the second quarter is slightly higher due to the slightly higher temperature, consequence both of convection heat transfer and exothermic heat released by the reactions happening in the first quarter. In the same way, around 130s, in the entire first half of the catalytic converter, solid

FIGURE 11 Solid temperature and CO mass concentration in time at different catalytic converter space positions with $T_S(t=0)=260K$, $\dot{m}_F=0.0043kg/s$ and $T_{Fin}=390K$ (a) and $T_{Fin}=410K$ (b).

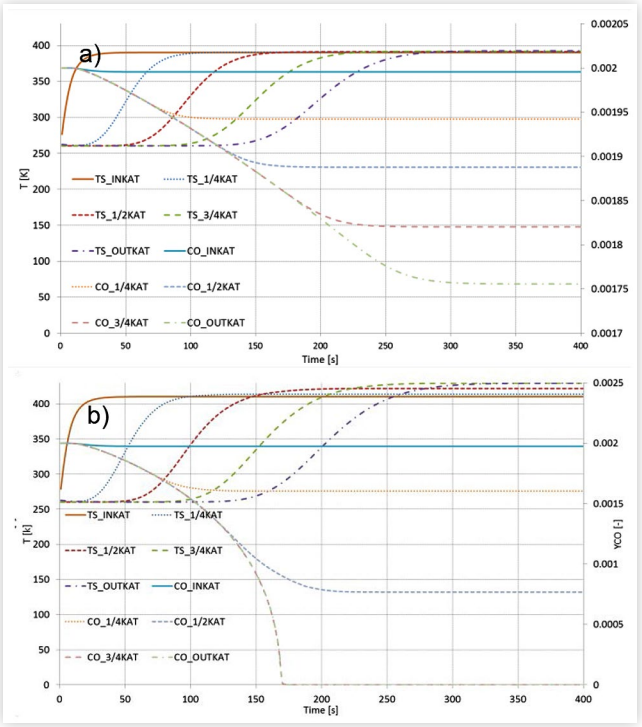

temperature, reaction rate and CO concentration have reached constant levels and reactions start in the third quarter.

In the first case with $TF_{in}=390K$, the conversion remains incomplete, CO is exiting the catalyst while the temperatures and the reaction rates are almost homogeneously distributed along the catalytic converter. On the contrary, at $T_{Fin}=410K$, the conversion is complete: the final temperature and the reaction rates increase along the catalytic converter and all the oxidation happens in the first three catalyst quarters.

Based on the computed CO concentrations by the detailed simulations, an evaluation for the simplification introduced by Eq. (24) can be assessed. Eq. (24) is formulated based on a stationary CO concentration on the solid surface. This means that the CO diffusion from the bulk flow to the solid walls

FIGURE 12 Detail of the first 150s of Fig. 11a.

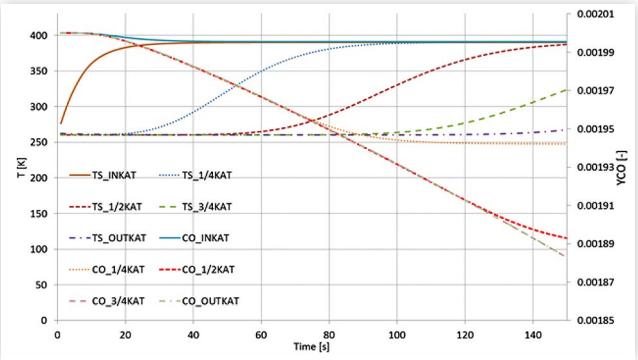

FIGURE 13 Comparison of the CO concentrations on the catalyst (solid) surface as computed by the detailed simulations and as obtained by assuming negligible temporal change and Eq. (24).

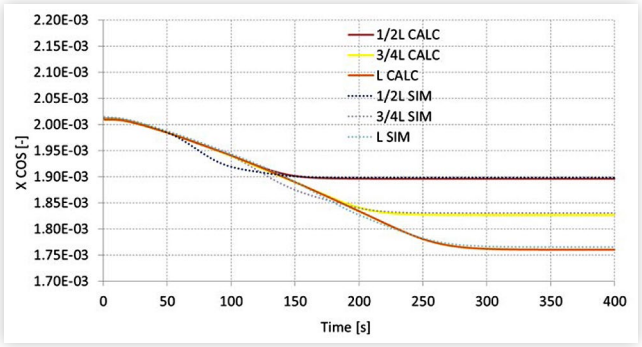

and the oxidation on the catalytic sites are in equilibrium and there is no temporal species accumulation on the surface. This assumption is questionable for the cold start, where temperature and concentration changes are rather high. The comparison shown in Fig. 13 hints, at least for the cases investigated in this study, that this assumption can be used without large deviations from the more detailed simulations.

In Fig. 14 results for the two different mass flows are compared. Here both CO inlet and outlet flowrates (on the left) and cumulative conversions (on the right) are plotted. The initial temperature of the exhaust ($T_{Fin}=390K$) and of the catalyst ($T_S=260K$) are identical for the two different mass-flows. The CO concentration in the inflow is identical, thus the double exhaust mass flow has also double amount of CO entering the catalyst. The conversions remain at a low level and the molar fraction of CO oxidized is similar in both cases. In fact, the variation in CO concentration is very similar for the two flowrates. This leads to much higher CO mass oxidized in the case of higher mass flowrate. But if we compare conversion efficiency, the higher value, (almost the double) is in the case of the low mass flow, around 12% while this is below 5% in the case of high mass flow. Conversions are overall low with both flow rates due to low inlet fluid and initial solid temperatures.

FIGURE 14 CO mass flow at the catalyst entrance and exit (on the right) and corresponding cumulative CO conversion (on the left) for two different exhaust mass flows (identical initial solid and inlet fluid temperatures).

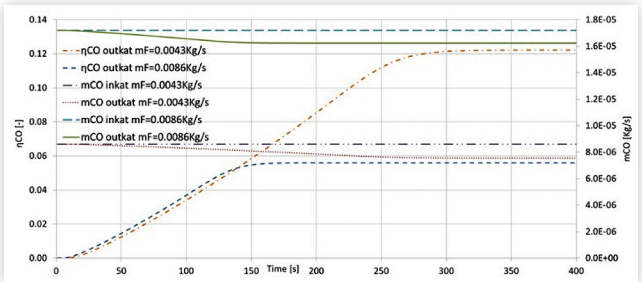

FIGURE 15 CO cumulative emissions in time with $T_S(t=0)$=(260, 300, 360)K, $\dot{m}_F$=0.0043kg/s and T_{Fin} =(373, 390,410, 425)K.

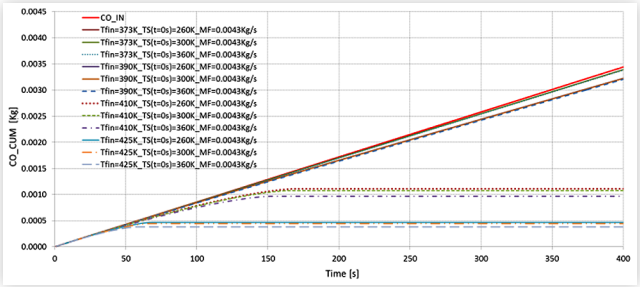

Evaluation of Possible Cold Start Emission Mitigation Strategies

Cumulative emissions are reported in Fig. 15 for the different configurations examined. In addition, the cumulative CO exiting the engine and entering the catalytic converter is reported (solid red) line. Independently of T_{Fin} and $T_S(t=0s)$, for the first 30s no reactions are happening and CO emissions consist of the linear, accumulation of the CO flowing in and out the catalyst. First deviations from the linear accumulation can be observed for the T_{Fin} =425K and $T_S(t=0)$=360K case, (highest fluid and solid initial temperatures). Later in time, reactions start in configurations with descending T_{Fin}. The most evident differences are noticed between cumulative emissions in the case of T_{Fin} =390K and of T_{Fin} =410K. For the case with T_{Fin} =425K, already after 50s CO is fully oxidized, while only after 150s when T_{Fin} =410K. The full conversion is not reached in the case of T_{Fin} =390K or T_{Fin} =373K. Considering the different $T_S(t=0s)$, the effect of higher $T_S(t=0s)$ reaches almost 30% in more conversion in the case of T_{Fin} =425K.

Based on these results, a preliminary and rough energetic assessment of possible means to accelerate the warm up can be obtained. The basic assumption is that the cold start occurs at an ambient temperature of $T_{amb}=T_S(t=0)$=260K and the first exhaust gas arriving from the engine has $T_{Engineout}$=373K. There are the following heating measures to compare: 1) the possibility of additionally heating the exhaust gas before the entrance of the catalyst and 2) the possibility of additionally heating the catalyst (solid) itself. The former can happen with the help of an electrical resistance, such systems are already exiting in the market, and the latter can be introduced with microwaves, as proposed in [2]. Sure, a possibility is to use a combination of both measures.

The energetic demand for heating up the exhaust gases to the discussed temperatures is summarized in Table 1. Assumed is a heating for 400s. As expected, the energy demand is proportional to the exhaust mass flow.

TABLE 1 Energy demand for heating up the exhaust gases from $T_{Engineout}$=373K to the different T_{Fin} for 400s.

T_{Fin}	[KJ] m_F=0.0043kg/s, Δt=400s	[KJ] m_F=0.0086kg/s, Δt=400s
390	29.50	59.01
410	64.21	128.43
425	90.24	180.49

The energetic demand for heating up the entire catalyst (solid) is summarized in Table 2:

TABLE 2 Energy demand for heating up the catalyst from T_S (t=0)=260K.

T_S	[KJ]
300	65.15
360	162.87

An easement of these measures has to be done on the basis of the energy needed in order to oxidize 1% additional CO. Taking into account the results shown in Fig. 13 and the energetic demands as shown in Tables 1 and 2, the results are summarized in Tables 3 and 4:

TABLE 3 Energy needed for an additional 1% CO oxidation $\dot{m}_F$=0.0043kg/s, T_S (t=0)=260K and $T_{Engineout}$=373K.

[KJ/%CO]	T_F=373K	T_F=390K	T_F=410K	T_F=425K
T_S=260K		3.9	0.4	0.3
T_S=300K	36.8	12.2	1.9	1.8
T_S=360K	77.6	22.5	3.2	2.8

TABLE 4 Energy needed for an additional 1% CO oxidation $\dot{m}_F$=0.0086kg/s, Ts(t=0)=260K and $T_{Engineout}$=373K.

[KJ/%CO]	T_F=373K	T_F=390K	T_F=410K	T_F=425K
T_S=260K		13.1	1.4	0.7
T_S=300K	60.2	28.3	3.0	1.5
T_S=360K	138.8	38.0	4.1	2.0

There are several conclusions to be drawn from Tables 3 and 4. For the exhaust mass flows investigated, preheating the exhaust gases leads to a higher extra oxidation with respect to the case of preheating the entire catalyst. At higher exhaust mass flows, this conclusion can change since the kJ/%CO at double the exhaust mass flow increases by a factor of almost 4 if preheating the exhaust gases, while only by a factor of 1.8 when heating only the catalyst. Heating the catalyst may be significantly more interesting when focusing not on the entire catalyst but only on a fraction of it in the upstream. Finally, a combination of the gas preheating and solid preheating has the potential to yield the best results.

Conclusions

In this study, the heat up of the catalytic converter during cold start has been analyzed using numerical simulation results. As a typical case, the flow of exhaust gases through a honeycomb catalyst (at lower temperature) has been simulated. For cold starts, typical, moderate exhaust gas temperatures have been chosen. Different setups in terms of fluid inlet temperatures, mass flow rates and catalyst initial temperatures have been compared.

As long as temperatures of the solid catalyst are at a level where chemical reactions are negligible, following insights can be summarized:

- The exhaust gas warms up the catalyst entrance and is cooled down to the catalyst initial temperature in the direct downstream.
- Temporal temperature gradients at the entrance are significantly higher than in the downstream. Thus, the entrance part of the catalyst reaches the gas inflow temperatures significantly faster than the downstream parts.
- Temperature differences between solid and fluid are larger at the entrance of the converter, significantly lower at the exit and decrease with time.
- The heat transfer between fluid and solid as well as the heat conduction in the solid is similar for the different cases investigated, i.e., for different mass flow rates, flow inlet and catalyst initial temperatures. The introduction of dimensionless temperature differences, dimensionless time and dimensionless space coordinates evidences the self similarity of the examined cases.
- The similarity of the heat transfer process results in similar heat-up patterns of different catalyst configurations. A larger catalyst heats up later in time but then at an accelerated rate.
- The catalyst heat up, expressed with the dimensionless parameters is, in all the cases examined, a double logarithmic function and can be approximated by a corresponding analytical expression, thus simplifying the solution of energy equation.
- For the cases examined, the highest heat transfer between fluid and solid occurred in the first catalyst part. Heat transfer rates were at 5W/m^3 and scaled with the fluid-solid temperature difference.

Consequently, first reactions occur in the entrance part of the catalyst. Should these produce significant heat, the warm up of the downstream parts of the catalyst is accelerated. The higher temperatures at the last portion of the catalyst are due to reactions happening in the first half of the catalytic converter, able to increase the solid and fluid temperature in the second half (convection) as well as due to local reactions.

- Higher $T_S(t=0)$ and or $T_{Fin}(t=0)$ reduce the time scales of the heat transfer, fasten and increase reactions rates.
- Higher $\dot{m}_F$ reduces the time scales of the heat transfer, but reduces reactions rates (in the temperature domain under investigation). The chemical time scales are too long while flow time scales too short.

The gains in CO oxidation based on the higher temperatures of either the exhaust gases or the solid are set in relation to the energy demand for the heating. In a preliminary assessment the conclusions are:

- Preheating the exhaust gases is more effective than preheating the entire solid catalyst, at the exhaust mass flows examined.
- This trend is reversed at higher mass flows.
- Preheating only the initial part of the solid has the potential to reach higher conversion for lower energy demand.

A final assessment can be delivered when taking into account the different heating mechanisms and their energetic efficiency as well as the associated energy generation in the propulsion system. In this work we presented mainly the tools which will allow more detailed assessments.

Nomenclature

T_{Fin}: - Inlet fluid temperature [K]

T_F: - Fluid temperature [K]

T_S: - Initial solid temperature [K]

T_0: - Reference temperature in dimensionless definitions [K], in this work the initial solid temperature was chosen.

x: - Dimensioned space coordinate [m]

t: - Dimensioned time coordinate [s]

L: - Catalytic converter length [m]

d: - Catalytic converter channel diameter [m]

ξ: - Dimensionless space coordinate [-]

ξ_i: - Dimensionless space coordinate for species i conservation equation [-]

τ: - Dimensionless time coordinate [-]

α: - Convection coefficient [W/(m^2 K)]

Λ: - Dimensionless solid conductivity [-]

$A_{//,}$ - Lateral Area [m^2]

$A_{S,FRONT}$ - Frontal Area [m^2]

$\dot{m}_F$: - Fluid mass flowrate [kg/s]

m_S: - Solid mass [kg]

S_v: - specific surface [1/m]

ε: - Solid porosity [-]

d_s: - strut diameter [m]

c: - specific heat capacity [J/(kg·K)]

c_p: - Isobaric specific heat capacity [J/(kg·K)]

Nu: - Nusselt number [-]

Pr: - Prandtl number [-]

$\lambda_{F:}$ - Fluid thermal conductivity [W/(mK)]

λs: - Solid thermal conductivity [W/(mK)]

$\rho_{s:}$ - Solid density [kg/m^3]

$\rho_{F:}$ - Fluid density [kg/m^3]

θ: - Dimensionless temperature difference [-]

u_∞ - Upstream velocity [m/s]

$\dot{q}_{conv}$: - convective heat per unit volume [J/m^3]

ΔV: - catalytic converter volume [m^3]

ΔH_R: - Heat of reactions [J]

q: - Heat rate exchanged per unit of catalyst volume[W/m^3]

C_{CO} : - molar concentration of CO [mol_{CO}/mol_{TOT}]

C_{O2} : - molar concentration of O2 [mol_{O2}/mol_{TOT}]

$\dot{n}_{co,i}$: - reacted material flow per unit of surface [$mol_{CO}/m^3/s$]

Kco: - mass transfer coefficient related to CO species [m/s]

Sh: - Sherwood number

$D_{CO:}$ - CO diffusion coefficient [m^2/s]

k_1: - Chemical reaction coefficient (Arrhenius formulation) [mol/(m^3 s)]

NTU: - Number of transfer unit [-]

E: - reaction activation energy [J/mol]

M_{CO} - CO molar mass [kg/mol]

M_F - Fluid molar mass [kg/mol]

δ: - control volume thickness where mass balance at the wall is applied [m]

$_S$: - Solid

$_F$: - Fluid

Acknowledgements

The authors gratefully acknowledge the Swiss federal Office for Environment for the project "Modellierung und Validierung des Katalysatorverhaltens bei Kaltstart und im Gesamtzyklus", contract no 15.0002.PJ / S122-1359, for the financial support. The authors acknowledge in addition, the axisuite software package which was used extensively for comparing the results of the detailed simulations

References

1. INFRAS, "Handbook Emission Factors from Road Transport (HBEFA) 3.2," 2014.
2. Papetti, V., Dimopoulos Eggenschwiler, P., and Schreiber D., "Reduction of Cold Start Emissions with Microwave Heated Catalytic converters," in *Proceedings of the 19th Stuttgart International Symposium, Automotive and Engine Technology*, 2019.
3. von Rickenbach, J., Lucci, F., Dimopoulos Eggenschwiler, P., and Poulikakos, D., Pore Scale Modeling of Cold-Start Emissions in Foam Based Catalytic Reactors, *Chem. Eng. Sci.* 138 (2015) 446-456. doi:10.1016/j.ces.2015.08.020.
4. Chen, D.K.S., Bissett, E.J., Oh, S.H., and Van Ostrom, D.L., "A Three Dimensional Model for the Analysis of Transient Thermal and Conversion Characteristics of Monolithic Catalytic Converters," SAE Technical Paper 880282, 1988, doi:10.4271/880282.
5. Koltsakis, G.C., Stamatelos, A.M., and Konstantinidis, P.A., "Development and Application Range of Mathematical Models for 3-Way Catalytic Converters," *Applied Catalysis B: Environmental*, 1997.
6. Votruba, J., Sinkule, J., Hlavacek, V., and Skrivanek, J., "Heat and Mass Transfer in Monolithic Honeycomb Catalysts-I," *Chem. Eng. Sci.* 30:117-123, 1975.
7. Koltsakis, G., "Warm-Up Behavior of Monolithic Reactors Under Non-Reacting Conditions," *Chem. Eng. Sci.* 53:2891-2899, 1997.
8. Sucec, J., "An Improved Quasi-Steady Approach for Transient Conjugated Forced Convection Problems," *Int. J. Heat Mass Transfer.* 24:1711-1722.
9. Della Torre, A., Montenegro, G., Onorati, A., and Cerri, T., "CFD Investigation of the Impact of Electrical Heating on the Light-off of a Diesel Oxidation Catalyst," SAE Technical Paper 2018-01-0961, 2018, doi:10.4271/2018-01-0961.
10. Peck, R.S., "Experimentelle Untersuchung und dynamische Simulation von Oxidationskatalysatoren und Diesel-Partikelfiltern," Ph.D. thesis, Institut für Chemische Verfahrenstechnik der Universität Stuttgart, 2007.
11. Voltz, S.E., Morgan, C.R., Liederman, D., and Jacob, S.M., *Ind. Eng. Chem. Prod. Res. Dev.* 12:294, 1973.
12. Tsinoglou, D.N., Eggenschwiler, P.D., Thurnheer, T., and Hofer, P., "A Simplified Model for Natural-Gas Vehicle Catalysts with Honeycomb and Foam Substrates," *P.I. Mech. Eng. D - J. Aut.* 223(6):819-834, June 2009.
13. Lucci, F., Della Torre, A., Montenegro, G., and Dimopoulos Eggenschwiler, P., "On the Catalytic Performance of Open Cell Structures versus Honeycombs," *Chem. Eng. J.* 264:514-521, 2015, doi:10.1016/j.cej.2014.11.080.
14. Incropera, F.P. and DeWitt, D.P., *Introduction to Heat Transfer* (New York: Wiley, 1996).
15. Oh, S.H. and Cavendish, J.C., "Transients of Monolithic Catalytic Converters: Response to Step Changes in Feedstream Temperature as Related to Controlling Automobile Emissions," *Ind. Eng. Chem. Prod. Res. Dev.* 21:29-37, 1982.

ISSN 0148-7191